

PAPER • OPEN ACCESS

## AURORA: a public applications server to introduce students to superconductivity

To cite this article: Nicolò Riva *et al* 2021 *J. Phys.: Conf. Ser.* **2043** 012005

View the [article online](#) for updates and enhancements.

You may also like

- [Cyclotron radiation emission spectroscopy signal classification with machine learning in project 8](#)

A Ashtari Esfahani, S Böser, N Buzinsky et al.

- [Spin dynamics in the pseudogap state: phase fluctuation versus  \$d\$ -density wave](#)

Hong-Min Jiang, Jian Zhou and Jian-Xin Li

- [Two-dimensional sample entropy: assessing image texture through irregularity](#)

L E V Silva, A C S Senra Filho, V P S Fazan et al.



The Electrochemical Society  
Advancing solid state & electrochemical science & technology

### 241st ECS Meeting

May 29 – June 2, 2022 Vancouver • BC • Canada

Extended abstract submission deadline: Dec 17, 2021

Connect. Engage. Champion. Empower. Accelerate.  
Move science forward



Submit your abstract



# AURORA: a public applications server to introduce students to superconductivity

Nicolò Riva<sup>1,2</sup>, Francesco Grilli<sup>3</sup>, Bertrand Dutoit<sup>1</sup>

<sup>1</sup>SCI IC BD, Ecole Polytechnique Fédérale de Lausanne, Lausanne, Switzerland

<sup>2</sup>MIT Plasma Science and Fusion Center, Cambridge, USA

<sup>3</sup>Institute for Technical Physics, Karlsruhe Institute of Technology, Karlsruhe, Germany

E-mail: nicoriva@mit.edu, francesco.grilli@kit.edu

**Abstract.** The growing interest in modeling superconductors has led to the development of increasingly effective numerical models and software. Alongside this interest, the question of how to teach and to explain the operation of superconductors to students has arisen. École Polytechnique Fédérale de Lausanne (EPFL) and Karlsruhe Institute of Technology (KIT) have created a series of web applications based on COMSOL Multiphysics that are publicly accessible through a web server called AURORA. Users can change the values of several parameters of the applications and observe the influence on the results. This article describes part of the currently available applications and some exercises that can be done with them.

## 1. Introduction

In confronting the growing necessity of innovative teaching methods, it is necessary to consider the needs of students and the educational system of today. Modern education is partially online, which opens new paths for the learning process.

In Roman mythology, Aurora was the goddess of the dawn who flew across the sky at sunrise, opening the path to the Sun and a new day\*. The server AURORA, presented in this paper, aims at opening the path to a new generation of brilliant students and ‘initiate’ them by learning superconductivity through Apps. The possibility of using applications for educational purposes allows demonstrating complex phenomena with a user-friendly interface. It also leverages a straightforward and visual teaching method to raise interest in students and allows them to have a glimpse at the potential impact that superconductivity can have in the world.

For this purpose, we have recently developed a series of applications to solve problems involving superconductors by means of finite-element method calculations. The applications are based on the commercial finite-element method software COMSOL Multiphysics [3] and focus on the electromagnetic and thermal behavior of superconductors at different scales. They range from the simulation of the penetration of quanta of magnetic flux (nanometer scale) to the simulation of the magnetic field in large magnets (meter scale).

\*See Virgil’s Aeneid, Book IV, verses 584-585 [1]: “Et iam prima novo spargebat lumine terras Tithoni croceum linquens Aurora cubile.” (Aurora’s young first beams were pouring as from Thithonus saffron bed she sprang [2].)



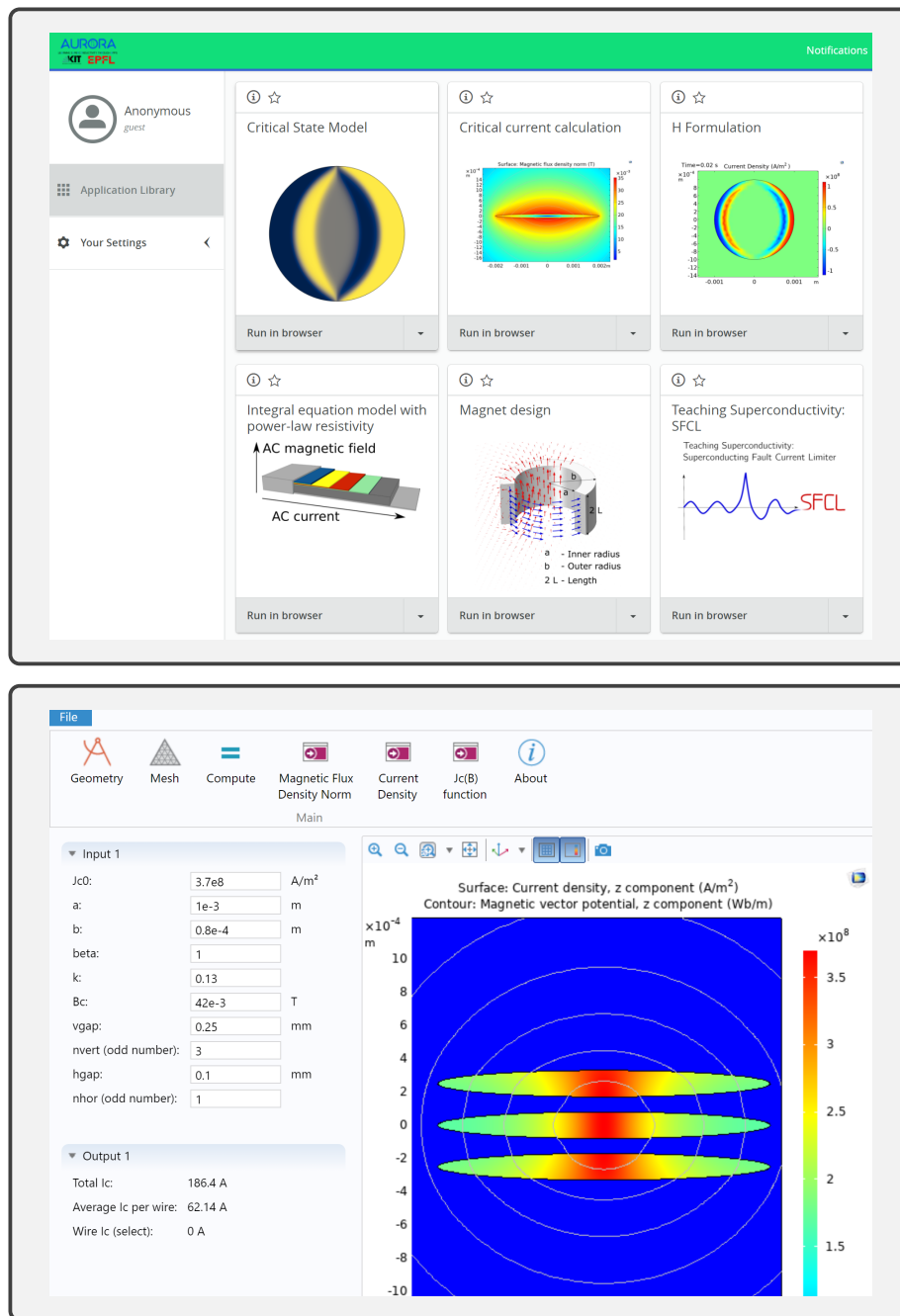


Figure 1: Web server user interface (top) and application user interface (bottom) for the *Critical Current Calculation* application.

With respect to the full-fledged version of the models implemented with the software, the applications available on the server have a simpler user interface. For each problem, the user can change a certain number of geometrical and physical parameters, and see how they affect the solution. In figure 1 (top) we present the web server user interface, which allows browsing and selecting the desired application. In figure 1 (bottom) we present how the initial interface for the critical current calculation application (section 2.6) looks like, with buttons to plot the geometry and the results (“Geometry”, “Compute”, “Current Density”, etc...). The parameters

can be changed in a tab menu on the left and additional information, including references to the literature, can be found by clicking the “About” tab.

The applications are publicly accessible with an internet browser. In this article we present a few selected applications currently available on the server and some example of how they can be used for exercises in the classroom.

## 2. Applications

### 2.1. Time-dependent Ginzburg-Landau equations

The goal of this application is to illustrate the dynamics of a superconducting sample in the presence of a magnetic field. This problem is solved by using the time dependent Ginzburg-Landau (TDGL) equations proposed by V. Ginzburg and L. Landau in 1950 [4]. Depending on a single parameter in the TDGL equations, the Ginzburg-Landau parameter  $k$ , the dynamics of superconductors in magnetic fields is that of a type-I (complete expulsion of the magnetic field, i.e. Meissner effect) or of a type-II superconductor (partial penetration of the magnetic field in the form of quantized vortices, i.e. mixed state). The problem is solved on a 2D superconducting disk with a geometric defect (figure 2) by using the TDGL equations coupled to a penetrating magnetic field  $\mathbf{B}_a$ . The dynamic behavior of the superconducting state in the TDGL equations is described by the order parameter  $\Psi = \Psi(x, y, t)$ . The parameter  $\Psi$  can be interpreted as the density of superconducting charge carriers (Cooper pairs) at position  $(x, y)$  and at time  $t$ : if  $|\Psi| = 1$  everywhere, the material is in a perfect Meissner state (zero magnetic field inside the superconductor), while if  $|\Psi| = 0$  everywhere, the field has fully penetrated and the material is no longer superconducting.

The normalized 2D TDGL equations under gauge transformation [4, 5, 6] read as follows:

$$\frac{\partial \Psi}{\partial t} = - \left( \frac{i}{k} \nabla + \mathbf{A} \right)^2 \Psi + \Psi - |\Psi|^2 \Psi, \quad (1)$$

$$\sigma \frac{\partial \mathbf{A}}{\partial t} = \frac{1}{2ik} (\Psi^* \nabla \Psi - \Psi \nabla \Psi^*) - |\Psi|^2 \mathbf{A} - \nabla \times \nabla \times \mathbf{A}, \quad (2)$$

with  $\sigma$  being the electrical conductivity,  $\mathbf{A}$  being the magnetic vector potential,  $i$  being the imaginary unit, and  $k = \lambda/\xi$  being the Ginzburg-Landau parameter, i.e. the ratio between the London penetration depth  $\lambda$  of the magnetic field and the Ginzburg-Landau coherence length  $\xi$  [4]. Note that also the time  $t$  and the vector potential  $\mathbf{A}$  are normalized, and their units are 1. The boundary conditions applied to the superconducting sample (normalized and under gauge transformation) are [6, 7]:

$$\nabla \Psi \cdot \mathbf{n} = 0, \quad \nabla \times \mathbf{A} = \mathbf{B}_a, \quad \mathbf{A} \cdot \mathbf{n} = 0, \quad \text{on } \partial\Omega, \quad (3)$$

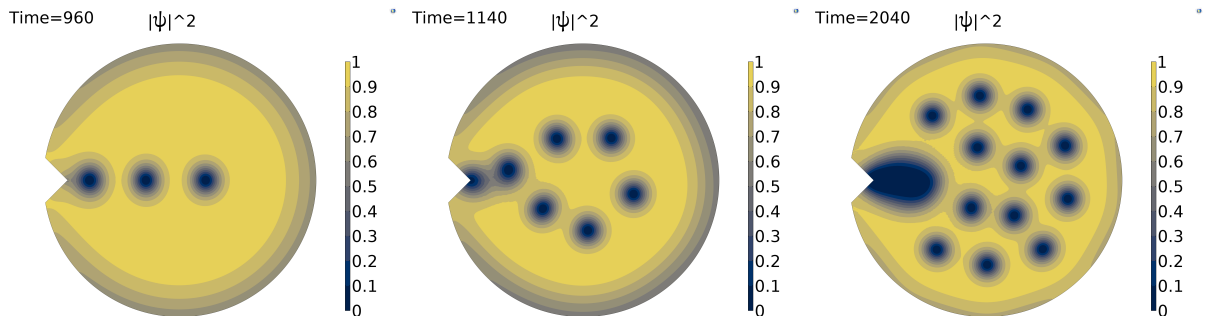


Figure 2: Absolute value  $|\Psi(x, y, t)|^2$  of the order parameter for  $k = 4$  and  $|\mathbf{B}_a| = 0.9 B_c$  at three different simulation normalized times ( $t_1 = 960$ ,  $t_2 = 1140$ ,  $t_3 = 2040$ ).

where  $\mathbf{B}_a = |\mathbf{B}_a|\mathbf{u}_z$  is the uniform external magnetic field along the  $z$ -axis direction (outward the paper),  $\partial\Omega$  is the boundary of the superconducting domain and  $\mathbf{n}$  the outward normal vector to the boundary.

In this application, equations (1) and (3) are solved using four time-dependent and coupled nonlinear partial differential equations (PDE module in COMSOL [3]). In figure 2 we present the results for an applied magnetic field of  $|\mathbf{B}_a| = 0.9 B_c$  (where  $B_c$  is the critical field) and  $k = 4$  (type II superconductor). In this figure, it is possible to visualize the dynamics of the magnetic flux entering at the defect ( $t = 960$ , figure left); the circular regions with  $|\Psi|^2 = 0$  indicate a vortex and a normal-conducting zone. For successive times ( $t = 1140, 2040$ ) multiple vortices enter the superconductor occupying gradually the entire superconductor.

The exercise allows modifying parameters such as the radius of the sample  $r_0$  (in units of  $\xi$ ), and the Ginzburg–Landau parameter  $k$  which determines whether a superconductor is type-I ( $0 < k < 1/\sqrt{2}$ ) or type-II ( $k > 1/\sqrt{2}$ ). In addition, it is possible to adjust the time length of the simulation  $t_{\text{end}}$  and the maximum normalized applied magnetic field  $B_a$ .

## 2.2. Critical state model

This application simulates the electromagnetic response of an infinitely long superconducting wire of elliptical cross section to a transverse sinusoidal external field using the simple critical state model (CSM) [8, 9], where the magnetic field penetrates via a screening current whose density can only be 0,  $+J_c$  or  $-J_c$ . For the implementation of the CSM, the method of the force–displacement curve of the flux lines proposed by A. M. Campbell is used [10].

This application simulates 1.25 cycles of an externally applied AC magnetic field and uses the magnetic vector potential  $\mathbf{A}$  (which in the 2D problem considered here is a scalar) as state variable. The current density and magnetic vector potential distributions at each considered instant are calculated starting from the results ( $J_p, A_p$ ) at the last point of inversion of the applied field – see figure 3.

The model consists in a parametric study of magnetostatic simulations (one for each calculated instant) solving the equation

$$\nabla \times (\nabla \times \mathbf{A}) = \mu_0 J_p + k \left[ 1 - \exp \left( - \left| \frac{(\mathbf{A} - \mathbf{A}_p) \mu_0 J_c}{k A_r} \right| \right) \right], \quad (4)$$

with

$$k = \mu_0 J_c \text{sgn}(\mathbf{A}_p - \mathbf{A}) - \mu_0 J_p. \quad (5)$$

In this way, the model is frequency-independent, as required by the CSM. The model is implemented in units of AC cycles; in figure 3, we kept the notation  $\omega t$  for practical purposes.

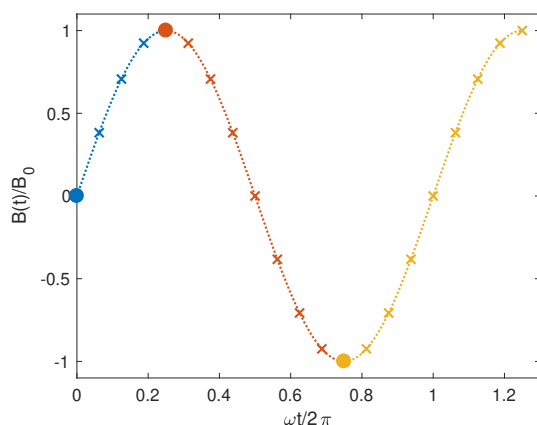


Figure 3: Applied magnetic field  $\mathbf{B}(t) = \mathbf{B}_0 \sin(\omega t)$ : according to equations (4-5), the solution at a given instant  $\omega t > \pi/2$  during an AC cycle (crosses) is calculated starting from the points of inversion ( $\omega t = \pi/2$  and  $\omega t = 3\pi/2$ ). For the points at  $\omega t < \pi/2$ , the instant  $t = 0$  is chosen as starting point and the equation to be solved takes a simpler form.

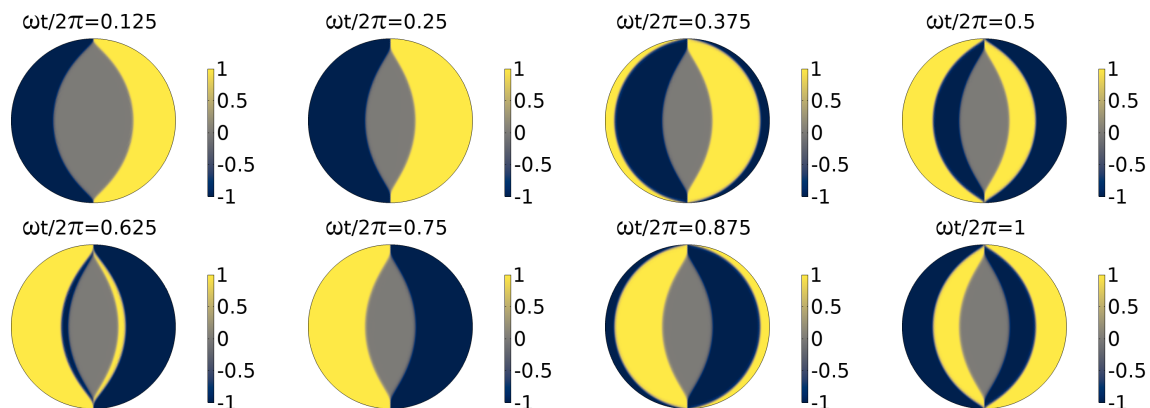


Figure 4: Normalized current density distributions ( $J/J_c$ ) in the cross section of an infinitely long circular wire subjected to a transverse field  $\mathbf{B}_0 \sin(\omega t)$ . The distributions refer to different instants of the first AC cycle.

The parameter  $A_r$  is the product of the magnetic flux density  $B$  and a characteristic distance related to the vortex spacing. In order to obtain CSM-like results,  $A_r$  needs to be sufficiently small (e.g.  $1 \times 10^{-8} \text{ Wb m}^{-1}$  for typical examples solved with this application).

Figure 4 shows the normalized current density distribution in a wire subjected to a transverse field  $\mathbf{B}_0 \sin(\omega t)$ . The distributions are taken at different instants of the AC cycle. In the application, users can change various parameters, such as the critical current density  $J_c$ , the eccentricity of the cross section of the wire, the magnitude and direction of the applied magnetic field. A possible exercise is to change the eccentricity of the superconductor, without changing its cross section and  $J_c$ , and see how the simple deformation of the geometry has a large impact on the AC losses. More details about this and the influence of the direction of the magnetic field on the AC losses can be found in sections 4.1-4.2 of [11].

### 2.3. $H$ formulation

This application solves a similar problem as the previous one, but using a power-law dependence of the resistivity on the current density instead of the CSM as a constitutive law of the superconducting material. The application is based on the  $H$  formulation, which solves Faraday's equation using the magnetic field  $\mathbf{H}$  as state variable

$$\frac{\partial(\mu\mathbf{H})}{\partial t} + \nabla \times (\rho \nabla \times \mathbf{H}) = 0 \quad (6)$$

and, according to the power law, uses a nonlinear resistivity for the electrical characteristic of the superconductor

$$\rho = \frac{E_c}{J_c} \left| \frac{\mathbf{J}}{J_c} \right|^{n-1}. \quad (7)$$

More details about the formulation can be found in [12, 13].

The application simulates a time-dependent problem. The use of the non-linear resistivity introduces a dependence of the results on the rate of change of the applied current and field. In particular, using lower  $n$  values in equation (7) or low frequencies in the external current and/or field excitations leads to different results. This is an important difference with respect to the CSM, whose results are rate-independent. An example is shown in figure 5, which displays the normalized current density distribution  $\mathbf{J}/J_c$  in a round wire carrying 80% of its critical current for different  $n$  values and frequencies. The first figure on the left represents a 'standard'

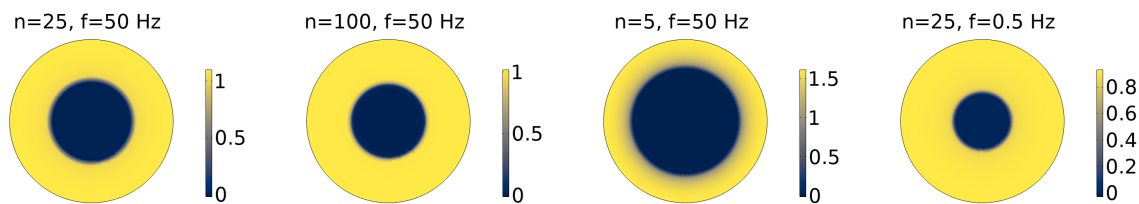


Figure 5: Normalized current density distributions ( $J/J_c$ ) in the cross section of an infinitely long circular wire carrying 80% of the critical current for different values of the power index  $n$  and frequencies. The distributions are taken at the peak of the AC cycle. Note the different scales of the color bar.

case, with  $n = 25$  and  $f = 50$  Hz: due to the finite value of  $n$ , regions with a current density value slightly exceeding  $J_c$  are allowed. A close inspection of the second figure from the left reveals that increasing  $n$  to 100 limits the maximum value of  $\mathbf{J}/J_c$  to values closer to one. This is because, as  $n$  increases, the power-law (7) approaches the critical state model. Conversely, if  $n$  is very low ( $n = 5$  in the third figure from the left) values of  $J$  greatly exceeding  $J_c$  are allowed: as a consequence, the area of the current-carrying region is much reduced. Finally, the last figure on the right shows that the current density tends toward sub-critical values, when the frequency of the transport current is reduced to 0.5 Hz. This is a phenomenon important in several HTS applications, for example HTS magnets, which are charged and discharged with slow current ramps.

#### 2.4. Integral equation model for a thin superconductor

This application uses an integral equation approach to simulate the same type of problems as the  $H$  formulation, but for an infinitely thin superconductor. This geometry can be used to simulate the superconducting layer of an HTS coated conductor, which is characterized by an extremely large width-to-thickness ratio. In practice, only a 1D domain is simulated. In addition, differently from the  $H$  formulation, the use of an integral equation for the state variable current density allows simulating only the superconductor's domain, without the need of simulating the vacuum around it. This greatly reduces the number of degrees of freedom of the problem. As with the  $H$  formulation, the superconductor is simulated as a material with nonlinear power-law resistivity – equation (7).

The infinitely thin conductor approximation presents some distinctive features, including sub-critical current densities in field free-regions [14, 15]. A visual representation of how this results as the limit of the current distribution in a rectangular conductor as its thickness approaches zero can be found in [16].

This applications allows simulating the same cases as the  $H$  formulation, but for the specific geometry of a thin superconductor. An example of simultaneous application of current and field is shown in figure 6. Shown there are the current density and the magnetic flux density distribution in an infinitely thin superconductor carrying AC transport current while subjected to an in-phase AC magnetic field. The figure refers to the peak instant. The superconductor is 12 mm wide, has a critical current of 360 A, and a power index  $n = 25$ . The AC transport current is 180 A and the external field 20 mT. The frequency is 50 Hz. The asymmetry of the current and magnetic field distribution is clearly visible. Also noticeable is the sub-critical current density ( $J < J_c$ ) in the regions not reached by the magnetic field.

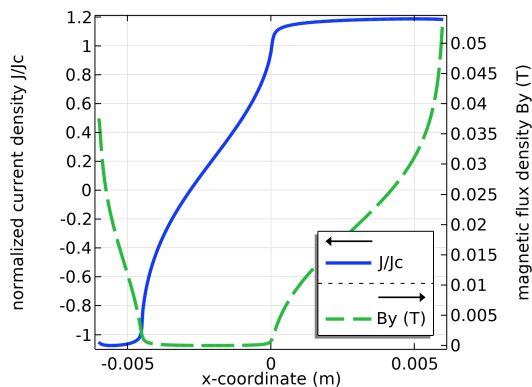


Figure 6: Current density and magnetic flux density distribution in an infinitely thin superconductor carrying AC transport current while subjected to an in-phase AC magnetic field. The figure refers to the peak instant.

### 2.5. Superconducting fault current limiter

A large-scale commercial usage of superconductor is the superconducting fault current limiter (SFCL) where the transition to normal state of a superconductor submitted to an overcritical current is used to protect a grid. This application allows investigating the electro-thermal response of an HTS coated conductor used in a resistive SFCL. The application solves a 1D thermal model coupled with a circuit representing the SFCL under AC fault conditions, evaluating important figures of merit such as the limited current, the prospective current and the maximum temperature reached within the tape. The circuit parameters, the geometrical parameters and the superconducting properties of the device can be modified. A detailed description of this application and of the model implementation can be found in a dedicated open-access publication [17], which also includes the discussion of four representative cases.

### 2.6. Critical current calculation

For certain high-current applications, it is necessary to bundle several tapes, in order to increase the current-carrying capacity. This application aims at showing the effects of self-field on the critical current of tape assemblies (like stacks and arrays), following the approach presented in [18]. In its simplest case, the applications simulates a wire of elliptical cross section, representing a Bi-2223 wire. The wire is considered to be infinitely long, so that it is sufficient to simulate a 2D cross section ( $xy$  plane). The current flows through the cross section and has thus only one component (in the  $z$  direction). The magnetic field has only the  $x$  and  $y$  components. It is assumed that the anisotropic dependence of the critical current density of the superconductor material on the magnetic flux density is a known function  $J_c(B_{\parallel}, B_{\perp})$ , where  $B_{\parallel}$  and  $B_{\perp}$  are the parallel and perpendicular components of the field with respect to the flat face of the wire, respectively. In the geometry considered here,  $B_{\parallel} = B_x$  and  $B_{\perp} = B_y$ . The  $J_c(B_{\parallel}, B_{\perp})$  function is a property of the superconductor material and is the input for the calculation. It takes the following form [19]:

$$J_c(B_{\parallel}, B_{\perp}) = \frac{J_{c0}}{\left(1 + \frac{\sqrt{k^2 B_{\parallel}^2 + B_{\perp}^2}}{B_{c0}}\right)^b}, \quad (8)$$

where  $B_{c0}$  expresses how fast  $J_c$  decreases with the amplitude of the magnetic field,  $k$  is the anisotropy factor, and  $b$  is a damping parameter.

The model assumes that the current density is at the critical value everywhere in the superconductor. The important point here is that this critical value is not uniform: it is lower where the magnetic field is higher, according to the  $J_c(B_{\parallel}, B_{\perp})$  function. The model solves a magnetostatic problem, calculating the (self) magnetic field distribution  $\mathbf{B}(x, y)$  consistent with



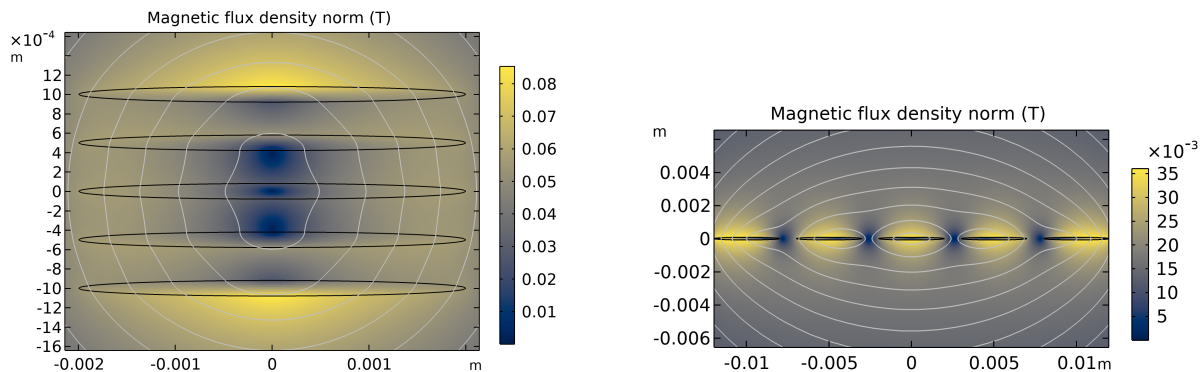


Figure 7: Magnetic flux density distribution in a vertical stack (left) and a horizontal array (right) of five elliptical wires.

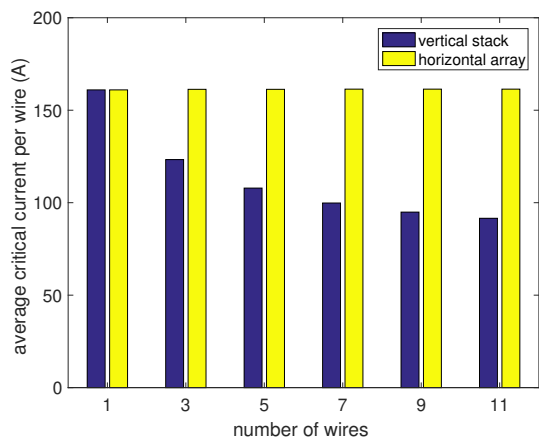


Figure 8: Average critical current per wire as a function of the number of wires composing the stack or the array. For the stack, the center-to-center distance is 0.5 mm; for the array, the edge-to-edge distance is 1 mm. The other parameters are:  $J_{c0} = 3.7 \times 10^8 \text{ A m}^{-2}$ ,  $B_{c0} = 42 \text{ mT}$ ,  $k = 0.13$ , and  $b = 1$ , which are typical for Bi-2223/Ag tapes at 77 K [20].

having  $J_c = J_c(\mathbf{B}(x, y))$  everywhere in the superconductor:

$$\nabla \times (\nabla \times \mathbf{A}) = \mu_0 J_c(\mathbf{B}(x, y)). \quad (9)$$

The effective critical current of the tape can be determined by integrating the  $J_c(\mathbf{B}(x, y))$  distribution over the superconductor's cross section.

The exercise is then extended to conductors composed of several tapes (stacks and arrays), in order to emphasize the influence of electromagnetic interaction between the tapes on the effective critical current of the composite conductors. An example is shown in figure 7, which displays the magnetic flux density distribution in a vertical stack (left) and a horizontal array (right) of five elliptical wires. Due to the compact arrangement of the wires and the resulting magnetic field, the critical current in the stack (539.5 A) is much lower than five times the critical current of the single wire (161 A). In the case of an array, the situation is very different: the wires are more distant from each other; in addition, in this arrangement the dangerous perpendicular component  $B_{\perp}$  is strongly reduced in the gap between the wires. This makes the critical current of the array equal (or even a little higher, 807 A) than five times the critical current of the single wire.

These effects depend on the number of wires and on their distance. Figure 8 shows the average critical current per wire as a function of the number wires composing the stack or the array. The decrease of the current-carrying capacity of the stack with increasing number of tapes is clearly visible. Conversely, the current-carrying capacity of the array is practically constant.

### 2.7. Magnet design

The biggest market for superconductors is magnets, in particular for nuclear magnetic resonance (NMR), magnetic resonance imaging (MRI), and particle accelerators. This application calculates the magnetic field distribution in solenoid-shaped magnet, modeled as a hollow cylinder with inner radius  $a$ , outer radius  $b$ , length  $2l$ . The user can modify the geometry of the magnet by adjusting the parameters  $\alpha = b/a$ ,  $\beta = l/a$ . Other input parameters are the uniform current density applied to the magnet's cross section and area of the wire's cross section used for the winding. The latter allows calculating the total length of the wire.

This application simulates the cross section of the magnet as a material characterized by a uniform current density. It can be used to show the influence of the magnet's shape on the uniformity of the magnetic field, which is a key parameter to determine the maximum current at which the superconductor can be operated.

In particular, this application can be used to carry out the exercises on magnet designs proposed in chapter 3 of [21] and chapter 7.4 of [22], with the visual aid of numerical simulations. In those exercises, the inner radius  $a$  and the target field  $B_0$  in the center of the solenoid are inputs of the problem. By using a field-dependent critical current density  $J_c(B)$  and the load-line method, it can be shown that the set of parameters  $\alpha, \beta$  corresponding to the minimum volume of conductor creates a magnetic field on the internal wall of the solenoid ( $r = a$ ) considerably higher than the target field  $B_0$ , which limits the current-carrying capability of the superconductor. An example is shown in figure 9. Other choices of  $\alpha, \beta$  can lead to a more uniform field and more efficient use of the superconductor, ultimately resulting also more economic.

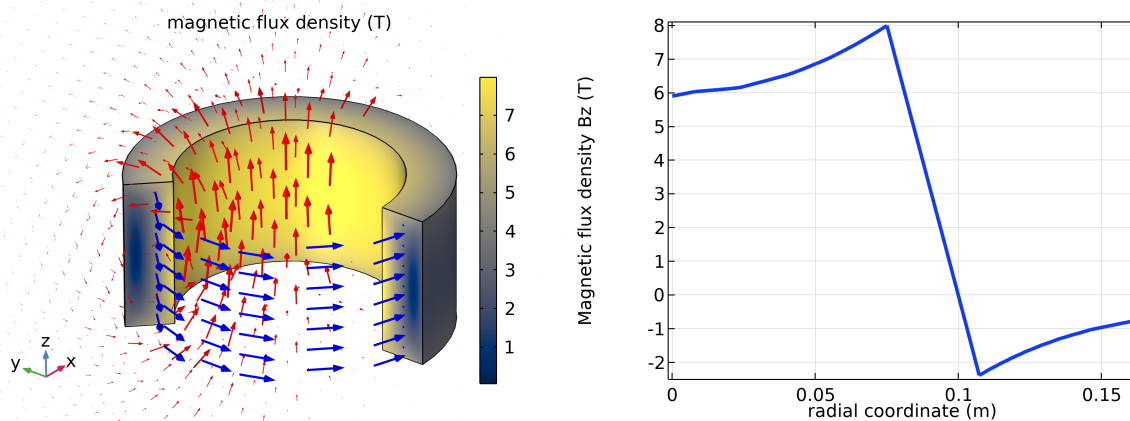


Figure 9: Magnetic flux density distribution in a solenoid. A uniform current density is assumed. This design is not suitable, because the magnetic field at the internal wall of the solenoid ( $r = 0.075$  m) is significantly higher than the target field in the center (about 8 T and 6 T, respectively).

### 3. Conclusion

We developed a series of applications for solving problems involving superconductors using finite-element method simulations implemented in COMSOL Multiphysics. The applications are publicly available on a server and accessible with a web browser. They solve different problems related to the electromagnetic and thermal behavior of superconductors. They are mainly directed, but not limited, to undergraduate students who want to learn more about superconductivity and its applications. This article presented a brief description of the applications currently available and of the type of exercises that it is possible to do with them.

We encourage interested users to contact the authors with proposals for improvement or for new applications.

### Acknowledgments

The authors would like to thank EPFL's IT team for providing the physical server where AURORA resides. The authors are also very grateful to Sven Friedel and Hinrich Arnoldt (COMSOL Multiphysics) and Ivar Kjelberg (CSEM SA) for their feedback and useful tips for the development of the various applications.

### References

- [1] *Virgil, Aeneid - Book IV verses 584-585* URL <https://www.thelatinlibrary.com/vergil/aen4.shtml>
- [2] *English translation of the verses 584-585* URL <http://www.perseus.tufts.edu/hopper/text?doc=urn:cts:latinLit:phi0690.phi003.perseus-eng2:4.584-4.629>
- [3] Finite-element software package COMSOL Multiphysics. <http://www.comsol.com>
- [4] Ginzburg V L, Landau L D, Leontovich M A and Fok V A 1950 *JETP* **20** 1064
- [5] Grishakov K S, Degtyarenko P N, Degtyarenko N N, Elesin V F and Kruglov V S 2012 *Physics Procedia* **36** 1206–1210
- [6] Alstrøm T, Sørensen M, Pedersen N and Madsen S 2006 The Ginzburg-Landau Equation Solved by the Finite Element Method *Proceedings of the Comsol Conference* ed Gregersen L (COMSOL Inc.) pp 75–78 ISBN 87-989426-1-1 Nordic Comsol Conference; Conference date: 01-01-2006
- [7] Alstrøm T S, Sørensen M P, Pedersen N F and Madsen S 2011 *Acta Applicandae Mathematicae* **115** 63–74
- [8] Bean C P 1962 *Physical Review Letters* **8** 250–252
- [9] Bean C P 1964 *Reviews of Modern Physics* **36** 31–39
- [10] Campbell A M 2007 *Superconductor Science and Technology* **20** 292–295
- [11] Grilli F and Rizzo E 2020 *European Journal of Physics* **41** 045203
- [12] Shen B, Grilli F and Coombs T 2020 *Superconductor Science and Technology* **33** 033002
- [13] Shen B, Grilli F and Coombs T 2020 *IEEE Access* **8** 100403–100414
- [14] Brandt E H and Indenbom M 1993 *Physical Review B* **48** 12893–12906
- [15] Zeldov E, Clem J, McElfresh M and Darwin M 1994 *Physical Review B* **49** 9802–9822
- [16] Grilli F, Abraham S and Brambilla R 2021 *Journal of Physics: Conference Series (in press)*
- [17] Riva N, Grilli F and Dutoit B 2021 *European Journal of Physics* **42** 045802
- [18] Gömöry F and Klinčok B 2006 *Superconductor Science and Technology* **19** 732–737
- [19] Zou S, Zermeño V M R and Grilli F 2016 *IEEE Transactions on Applied Superconductivity* **26** 8200705
- [20] Grilli F, Sirois F, Zermeño V M R and Vojenčiak M 2014 *IEEE Transactions on Applied Superconductivity* **24** 8000508
- [21] Wilson M N 1983 *Superconducting Magnets* (Clarendon Press Oxford)
- [22] Sharma R G 2015 *Superconductivity – Basics and Applications to Magnets* (Springer)